MATERIALS CHEMISTRY FRONTIERS

RESEARCH ARTICLE

View Article Online
View Journal

Cite this: DOI: 10.1039/d6qm00159a

Activating circularly polarized luminescence through environment-modulated polymorphic assembly of glycerolipid-modified carbazolyl phthalonitriles

Chuanqing Lan,[a] Xiao Chen,[a] Qingshuang Zou,[a] Zhiqi Liu,[b] Liwen Jiang,[b] Zhifeng Huang[a] and Dennis K. P. Ng*[a]

Received 28th February 2026,
Accepted 19th May 2026

DOI: 10.1039/d6qm00159a

rsc.li/frontiers-materials

Lipid molecules can self-assemble to form various supramolecular structures due to lipid polymorphism. Based on this property, conjugation of functional dyes with lipids can form a wide range of nanostructures with intriguing properties that have potential applications in various disciplines. In particular, materials that exhibit circularly polarized luminescence (CPL) are of much current interest. We report herein a simple molecular design of luminophore–glycerolipid conjugates, which can be molecularly engineered to induce CPL activity through changing the self-assembled environments. It involves an amphiphilic lipid chain substituted with a tris(carbazolyl)phthalonitrile moiety at the chiral center. With only one lipid chain, one polar head, one chiral center, and one luminophore, these molecules undergo self-assembly on a polar glass surface, on a nonpolar polydimethylsiloxane surface, and in water, leading to the formation of lipid nanocones, nanohemispheres, and nanotubes, respectively. Interestingly, while the latter two were CPL silent, the lipid nanocones could emit CPL with a significant luminescence dissymmetry factor of 0.01.

Introduction

Circularly polarized luminescence (CPL) has emerged as a critical phenomenon in the rapidly growing field of chiral photonics.[1,2] This unique feature producing light with a specific handedness has driven significant advancements in a variety of applications, such as optoelectronic displays,[3] bioimaging,[4] information encryption,[5–7] and asymmetric photochemical reactions.[8,9] The ability of chiral systems to emit CPL has garnered considerable attention due to its potential to revolutionize these technologies. Broadly, CPL-active materials are classified into two primary categories, namely chiral luminophores, which possess an intrinsically chiral molecular structure,[10–14] and achiral luminophores, which acquire chiral emission through self-assembly into supramolecular chiral structures.[15,16] A notable example of chiral luminophores is helically structured organic molecules, which exhibit CPL due to their inherent molecular chirality.[17,18] On the other hand, self-assembled CPL-active systems often involve supramolecular strategies to form chiral structures, such as chiral cages,[19] double helical π-aggregates,[20] helical microtoroids,[21] and chiral covalent organic frameworks.[22] The assembly of these materials offers a cost-effective and versatile approach to achieve CPL, as it relies on molecular packing and surface interactions to induce chiral order, circumventing the need for labor-intensive and expensive synthesis of chiral molecules. However, while these self-assembled systems are promising, challenges remain in optimizing the efficiency of CPL generation and controlling the specific chiral packing required for consistent performance. Advances in the understanding of the structure–activity relationship in these self-assembled CPL-active nanostructures are crucial for further development, which is still an active area of ongoing research.

Among the various classes of amphiphiles that can form supramolecular structures in aqueous media, amphiphilic lipids are of particular interest due to their unique ability to self-assemble into a variety of supramolecular architectures, such as liposomes, lipid nanoparticles, micelles, and bilayers, thanks to their adjustable hydrophilic–hydrophobic balance.[23,24] This intrinsic polymorphism allows for versatile design and fabrication of a wide range of functional lipid-based nanosystems for various applications, such as drug delivery, biosensing, and fluorescence imaging.[25–27] It is expected that the analogues with chiroptical properties could further advance the applications of these materials. To date, a number of CPL-active lipid-based

[a] Department of Chemistry, The Chinese University of Hong Kong, Shatin, N.T., Hong Kong, China. E-mail: dkpn@cuhk.edu.hk
[b] School of Life Sciences, The Chinese University of Hong Kong, Shatin, N.T., Hong Kong, China

materials have been reported, in which the luminophores are either covalently conjugated to the lipid components[28–30] or physically embedded in a chiral lipid-based supramolecular scaffold.[31–33] While most of these materials are based on cholesterol[34,35] or glutamate-based lipids,[36,37] glycerol-based lipids represent another promising class of lipid components. In particular, being the major building blocks of cell membranes, phospholipids constitute a key subject in homochirality research,[38] as in the case of amino acids. However, reports on CPL materials derived from glycerolipids remain scarce due to various challenges. Firstly, the glycerol backbone contains only one point-chiral center, which offers limited chirality amplification during supramolecular assembly, compared to the systems with axial chirality.[39] In addition, the self-assembly of glycerolipids relies predominantly on hydrophilic–hydrophobic interactions, lacking stronger intermolecular forces such as hydrogen bonding and π–π stacking.[40] As a result, they usually exhibit low phase transition temperatures, which can lead to collapse of the chiral supramolecular structures.[41] It is worth noting that not all chiral lipid-based systems are capable of generating CPL, and the molecular and supramolecular factors that determine the CPL generation efficiency remain elusive. Further research is needed to address these issues and improve the efficiency and stability of CPL emission in lipid-based supramolecular structures, making them more viable for practical applications.

To this end, we report herein a simple molecular design of luminophore–glycerolipid conjugates that can self-assemble into different supramolecular structures to give different CPL activity. It involves an amphiphilic lipid chain substituted with a tris(carbazolyl)phthalonitrile (Cz_3PN) moiety at the chiral center (Fig. 1a). Carbazolyl phthalonitrile derivatives are well known for their thermally activated delayed fluorescence (TADF), aggregation-induced emission characteristics, and high photoluminescence quantum yields, making them attractive candidates for optoelectronic, photocatalytic, and sensing applications.[42,43] Through lipid conjugation, which provides an effective strategy to introduce chiral environments, the CPL activity of these molecules can be modulated *via* controlled self-assembly. In contrast to the previously reported CPL-active lipid-based systems,[28–37] this enantiomeric pair of conjugates contains only one lipid chain, one polar head, one chiral center, and one luminophore, which can self-assemble without the need for other lipid components. These single-component self-assembled nanosystems can facilitate the study of structure–activity relationship and modulation of the CPL activity. Specifically, the self-assembly of these molecules on a polar glass surface, on a nonpolar polydimethylsiloxane (PDMS) surface, and in water led to the formation of lipid nanocones, nanohemispheres, and nanotubes, respectively (Fig. 1b). Only the lipid nanocones on the glass surface could emit CPL with a notable luminescence dissymmetry factor (g_{lum}) of 0.01. The results are reported and discussed in detail below.

Results and discussion

Synthesis and characterization

Scheme 1 shows the synthetic pathway used to prepare these enantiomeric Cz_3PN-modified glycerolipids. Treatment of cetyl alcohol (**1**) with optically pure (*R*) or (*S*)-epichlorohydrin (**2**) in the presence of NaOH and tetrabutylammonium bromide (TBAB) afforded the substituted products **3** in excellent yield. By measuring the plane-polarized light rotation angles of these compounds and making reference to those of optically pure (*R*)-(−) and (*S*)-(+)-2-(hexadecyloxymethyl)oxirane reported previously,[44] it was found that the reactions proceeded predominantly *via* epoxy ring opening followed by intramolecular

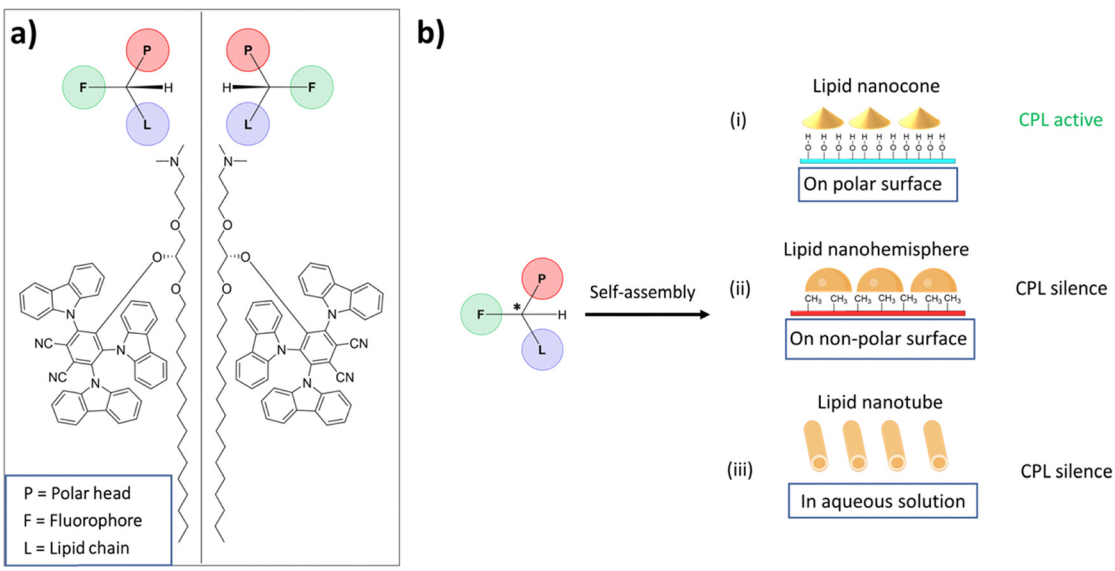

Fig. 1 (a) Molecular structures of the enantiomeric Cz_3PN-modified glycerolipids. (b) Self-assembly of these lipid molecules on a polar glass surface, on a nonpolar PDMS surface, and in water forming different supramolecular structures with different CPL activities.

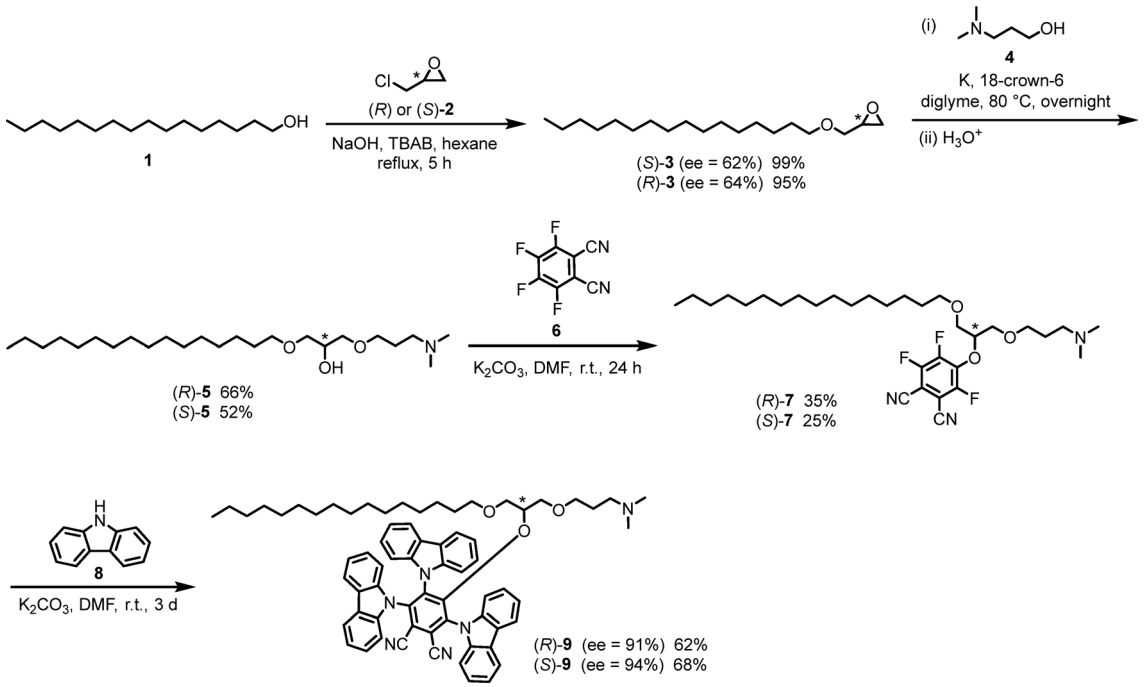

Scheme 1 Synthesis of enantiomeric Cz_3PN-modified glycerolipids (*R*) and (*S*)-**9**.

substitution instead of direct displacement of the chloro leaving group, leading to inversion of the chiral center with an enantiomeric excess (ee) of *ca.* 60%. These enantiomeric mixtures were then treated with 3-dimethylamino-1-propanol (**4**), using potassium with 18-crown-6 to facilitate deprotonation of the hydroxy group. The reactions resulted in attack likely at the less substituted epoxide carbon by the alkoxide formed, leading to the formation of alcohols **5** with retention at the chiral center. These compounds were then separately treated with tetrafluorophthalonitrile (**6**) in the presence of K_2CO_3 to afford the corresponding mono-β-substituted products **7** as indicated by the appearance of three doublets of doublets for the three fluoro groups.[45] Further nucleophilic aromatic substitution of the remaining fluoro groups with carbazole (**8**) resulted in the formation of the target conjugates. To enhance the optical purity, the resulting enantiomeric mixtures were crystallized from hexane/$CHCl_3$ to give (*R*) and (*S*)-**9**, respectively, based on the fact that the chirality should be retained in the last two steps. Chiral high-performance liquid chromatography (HPLC) analysis revealed that these enantiomers were optically pure with an ee of 91% and 94%, respectively (Fig. S1), showing that enantioenrichment could be achieved through crystallization.[46] All the new compounds were characterized using various spectroscopic methods. The experimental details are reported in the SI.

The optical properties of (*R*) and (*S*)-**9** were first studied in *N*,*N*-dimethylformamide (DMF), a good solvent that can disperse the molecules of these compounds. Both of them exhibited a broad absorption with a maximum at *ca.* 330 nm (Fig. S2), which could be attributed to the Cz_3PN chromophore.[47] Upon excitation at 320 nm, they emitted fluorescence at *ca.* 550 nm (Fig. S3). The fluorescence lifetime was measured by time-correlated single photon counting, giving a value of 3.3 ns for both compounds (Fig. S4). As expected, both compounds did not give circular dichroism (CD) and CPL signals due to their well-dispersed and non-chiral state (Fig. S5 and S6, respectively). Their virtually identical optical properties were also expected due to their enantiomeric relationship.

Self-assembly and spectral properties in aqueous media

The self-assembly properties of the enantiomeric (*R*) and (*S*)-**9** in aqueous media were then studied using a nanoprecipitation method. To ensure the reproducibility and enhance the stability of the resulting nanostructures, a microfluidic Y-shaped chip was used to mix a solution of these compounds in ethanol (100 μM) at a flow rate of 100 μL min^{-1} with citrate buffer (50 mM, pH 4.0) at a flow rate of 500 μL min^{-1} at room temperature. The key parameters of the microfluidic chip provided by the manufacturer are given in Fig. S7. Dynamic light scattering (DLS) study revealed that the resulting nanoparticles exhibited a hydrodynamic diameter of *ca.* 220–230 nm (Fig. S8). To further examine the nanostructures, cryo-transmission electron microscopy (TEM) was used to image the nanostructures and determine their dimensions. As shown in Fig. 2a and b, these enantiomers self-assembled into nanotubes with a length of *ca.* 230 nm, which was consistent with the DLS data, a diameter of 20–22 nm, and a thickness of 5–6 nm, which was typical for lipid bilayers.[48]

After measuring the basic structural parameters, the spectral properties of these lipid nanotubes were investigated and compared with those of the free molecules generated by adding 1% Triton X-100 to disrupt the aggregates. Fig. 2c shows the

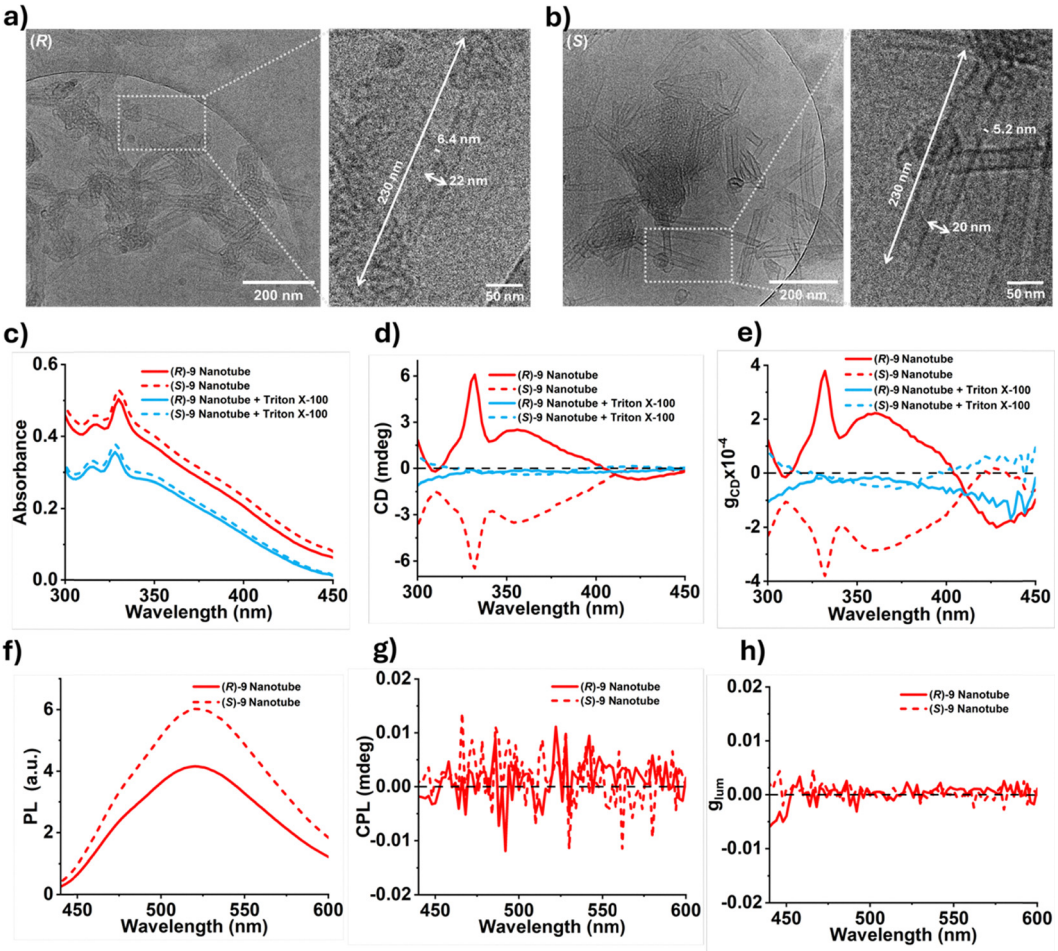

Fig. 2 Cryo-TEM images of the nanotubes of (a) (*R*)-**9** and (b) (*S*)-**9**. (c) Electronic absorption spectra, (d) CD spectra, and (e) absorption asymmetry factor (g_{CD}) of the nanotubes of (*R*) and (*S*)-**9** with or without the addition of 1% Triton X-100. (f) PL spectra (λ_{ex} = 320 nm), (g) CPL spectra, and (h) luminescence dissymmetry factor (g_{lum}) of the nanotubes of (*R*) and (*S*)-**9**. The concentration of the Cz_3PN unit was fixed at 20 μM for all the cases.

electronic absorption spectra of these systems. All of them displayed notable absorption bands at *ca*. 320–330 nm arising from the Cz_3PN chromophore,[47] in a strong scattering background, particularly for the lipid nanotubes. The spectra recorded in the presence of 1% Triton X-100 resembled those measured in DMF (Fig. S2), supporting the dissociation of the nanoaggregates. These absorption bands were not significantly shifted upon disassembly of the nanostructures, showing that the stacking environment of the chromophoric units remained essentially unchanged upon disassembly. As shown in Fig. 2d, the nanotubes of (*R*)-**9** exhibit two positive CD bands at approximately 330 and 355 nm, along with a weak negative feature at ~420 nm. Upon inversion of handedness to (*S*)-**9**, the CD spectrum becomes approximately mirror-symmetric with respect to the zero line. However, the signal at ~420 nm is significantly attenuated and is not clearly resolved in the (*S*)-enantiomer. This deviation from ideal mirror symmetry likely reflects the intrinsically weak chiroptical response of the lower-energy charge-transfer (CT) transition and its sensitivity to subtle differences in supramolecular organization, rather than solely instrumental or baseline offsets. For the molecular counterparts, these effects vanished, as the Cz_3PN chromophore that is responsible for these absorptions is achiral. This clearly indicates that the originally non-chiral chromophore acquires point chirality upon conjugation to a chiral lipid chain, and upon self-assembly, the molecules transfer their point chirality to the entire supramolecular structure, causing the chromophoric units to exhibit a chiral activity. The absorption asymmetry factors (g_{CD}) were also determined for both types of nanotubes (Fig. 2e). The values (up to 4×10^{-4}) were relatively small compared with those of materials based on other lipids.[49,50]

After studying the chirality of the nanotubes in the ground state of the molecules, we examined their excited state properties. As shown in Fig. 2f, a photoluminescence band at 525 nm was clearly observed for the nanotubes of (*R*) and (*S*)-**9** upon excitation at 320 nm. The weak shoulder at 475 nm may be attributed to trace amounts of isomeric impurities of carbazole that are commonly found in commercial samples.[51] Their fluorescence lifetimes were determined to be 3.5 ns by time-correlated single photon counting, which was comparable with that recorded in DMF (3.3 ns) (Fig. S4). Unfortunately, the

CPL signals were not noticeable, and the g_{lum} values could not be determined (Fig. 2g and h).

Self-assembly behavior on polydimethylsiloxane and glass

Considering the polymorphism of lipid molecules, their self-assembled forms can be altered, which may provide a mechanism to alter the CPL activity of (*R*) and (*S*)-**9**. Hence, we selected a solid substrate to establish an air–solid interfacial environment for the molecules to align. Owing to the distinct interfacial properties of solids, the use of different solid substrates enables tuning of the environment that can modulate the molecular packing and eventually their chiral properties. Specifically, polydimethylsiloxane (PDMS) and glass were employed to approximate air–nonpolar and air–polar interfaces, respectively. A solution of (*R*) or (*S*)-**9** in ethanol (1 mM, 30 μL) was deposited onto PDMS and glass substrates. After solvent evaporation, the resulting films were analyzed using atomic force microscopy (AFM) (Fig. 3). In both cases, nanoscale assemblies were observed, suggesting that Cz_3PN-modified glycerolipid molecules are capable of organizing into discrete structures on these substrates. The lateral dimensions of the assemblies were broadly distributed in the range of ∼400–600 nm, while their heights varied depending on the substrate. Specifically, features on PDMS exhibited heights of ∼30–50 nm, whereas those on glass appeared taller, typically ∼80–100 nm (Fig. 3a and b). This apparent substrate-dependent height difference may be influenced by variations in interfacial wetting, spreading behavior, and solvent evaporation dynamics, although contributions from tip-sample interactions and substrate-induced deformation cannot be excluded.[52] Statistical analyses of the AFM images (Fig. S9 and S10) indicate that the structures shown in Fig. 3 are representative of the predominant features under the examined conditions.

To further examine morphology, AFM data were processed using edge detection and three-dimensional (3D) reconstruction (Fig. 3c and d). The assemblies formed on PDMS appear dome-like, whereas those on glass exhibit more tapered or cone-like profiles. However, given the known limitations of AFM in resolving steep or high-aspect-ratio features, these shape assignments should be interpreted with caution. Higher-magnification 3D renderings reveal surface textures on the cone-like structures that may suggest a degree of structural anisotropy (Fig. 3e). Differences observed between assemblies derived from (*R*) and (*S*)-**9**, including apparent opposite twisting features and scan-direction-dependent contrast, are consistent with a mirror-symmetric relationship. Nevertheless, while these textures could be indicative of supramolecular chirality, alternative explanations, such as imaging artifacts, tip convolution effects, or reconstruction-induced distortions, should also be considered.[53]

To probe possible substrate–molecule interactions, Raman spectra of the assemblies were compared with those of the bare substrates (Fig. S11). No significant shifts were observed in the ν_{O-H} band of glass (∼3270 cm^{-1}) or the ν_{C-H} bands of PDMS (∼2900 cm^{-1}) after deposition. While this may suggest that strong specific interactions (*e.g.*, O–H···N hydrogen bonding) are not dominant, the absence of detectable spectral shifts does not definitively rule out more subtle or localized interactions. Overall, the self-assembly process is likely influenced by a combination of hydrophobic effects and interfacial factors, although the relative contributions of these interactions remain to be fully elucidated.

Spectral properties on polydimethylsiloxane and glass

After elucidating the nanostructures of these interfacial self-assemblies, we next investigated their spectroscopic properties. The films were mounted on a solid sample holder, and CD signals were recorded by averaging measurements at rotation angles of 0°, 90°, 180°, and 270° to minimize artifacts arising from linear dichroism. For CD and CPL measurements, the film planes were oriented perpendicular and at 45° to the optical path, respectively. As shown in Fig. 4a, the absorption spectra of the nanohemispheres and nanocones closely resemble those of the nanotubes, with a prominent band at ∼330 nm attributed to the Cz_3PN chromophore. The CD spectra of the nanocones derived from (*R*) and (*S*)-**9** exhibit approximate mirror symmetry, similar to the nanotubes (Fig. 4b), but display markedly enhanced Cotton effects at ∼420 nm. In contrast, although the nanohemispheres of (*R*) and (*S*)-**9** also show mirror-image CD profiles, the symmetry axis is slightly offset from zero, and the dominant Cotton effect likewise appears at ∼420 nm. As summarized in Fig. 4c, the g_{CD} values for the nanocones are 1.0, 0.5, and 0.5 ($\times 10^{-4}$) at 330, 355, and 420 nm, respectively, whereas the corresponding values for the nanohemispheres are 0.1–0.2, 0.1–0.2, and 2.0 ($\times 10^{-4}$). These results highlight the strong dependence of chiroptical properties on the specific nanostructure.

For carbazolyl phthalonitrile derivatives, the absorption band at ∼330 nm is generally assigned to the localized π–π* transition of the carbazole unit, whereas the longer-wavelength bands (∼350–420 nm) are associated with transitions of increasing CT character.[54–56] In donor–acceptor-type TADF systems, these CT transitions are highly sensitive to the dihedral angle between donor and acceptor moieties. Based on previous studies, including that of understanding complex spin up-conversion processes in CT-type organic molecules, the band near 355 nm can be interpreted as a transition with mixed local excited (LE) and weak CT character, consistent with limited donor–acceptor orbital overlap (*e.g.*, near-orthogonal geometries), whereas the ∼420 nm band reflects a more delocalized CT state enabled by increased conjugation. On this basis, the CD spectra of the different nanostructures of **9** provide insight into supramolecular organization. Lipid nanotubes exhibit strong, mirror-symmetric CD signals at 330 and 355 nm, with minimal contribution at 420 nm, suggesting predominantly weakly coupled LE/CT states arranged in a chiral fashion. Lipid nanocones display CD signals across all three bands, indicating coexistence of multiple conformations. In contrast, lipid nanohemispheres show dominant CD at 420 nm, consistent with enhanced CT delocalization, while reduced signals at shorter wavelengths may arise from partial cancellation of chiroptical responses due to increased conformational heterogeneity.

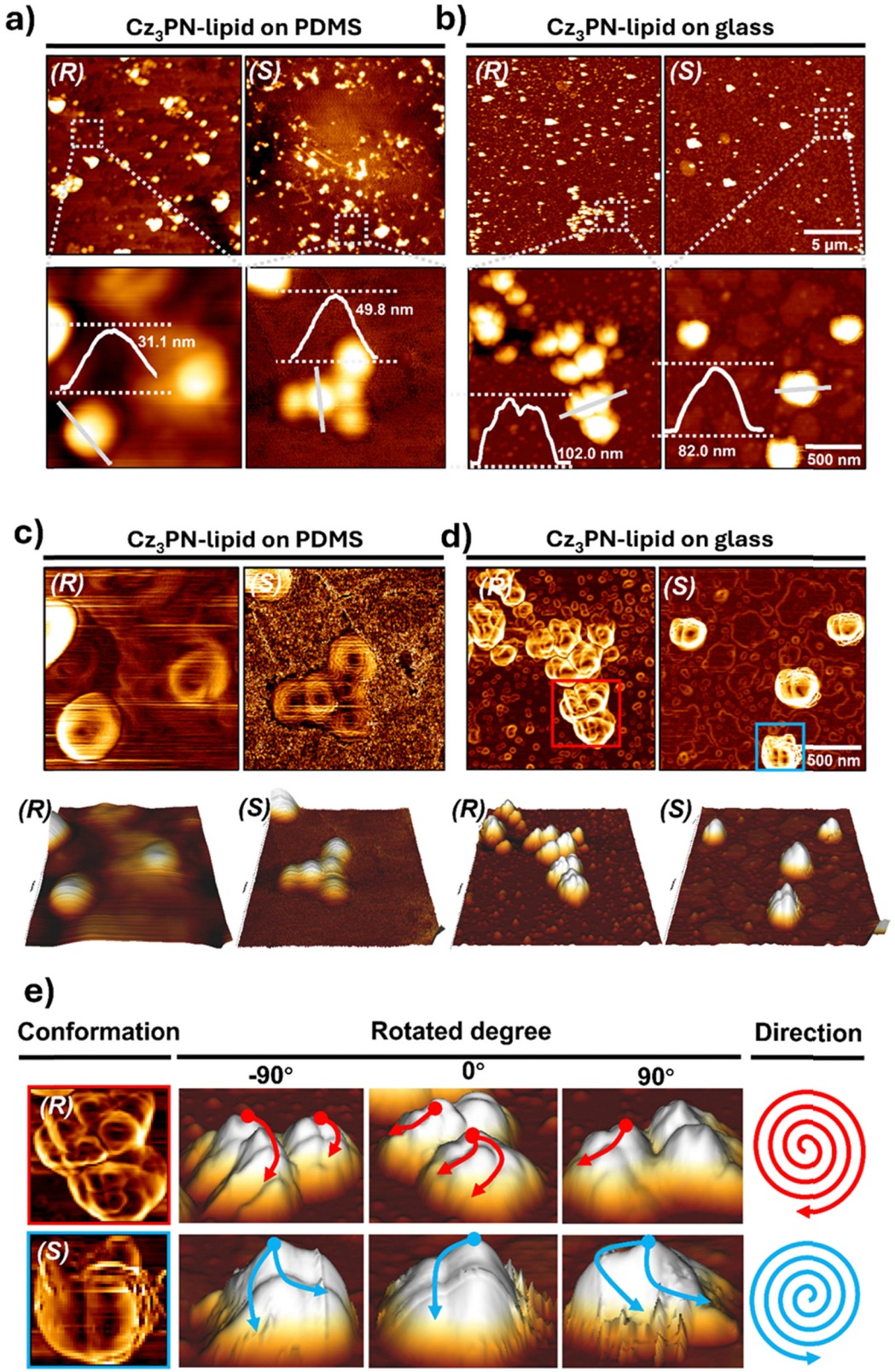

Fig. 3 AFM images of the nanostructures of (*R*) and (*S*)-**9** formed on (a) PDMS and (b) glass. Magnified images and the height of selected nanostructures are shown in the lower row. (c) AFM images of the nanohemispheres of (*R*) and (*S*)-**9** formed on PDMS viewed by edge detection (upper row) and 3D view (lower row). (d) Corresponding images of the nanocones of (*R*) and (*S*)-**9** formed on glass. (e) AFM images of enlarged nanocones of (*R*) and (*S*)-**9** formed on glass viewed by edge detection (left-most column) and 3D view with different rotation degrees (the other three columns).

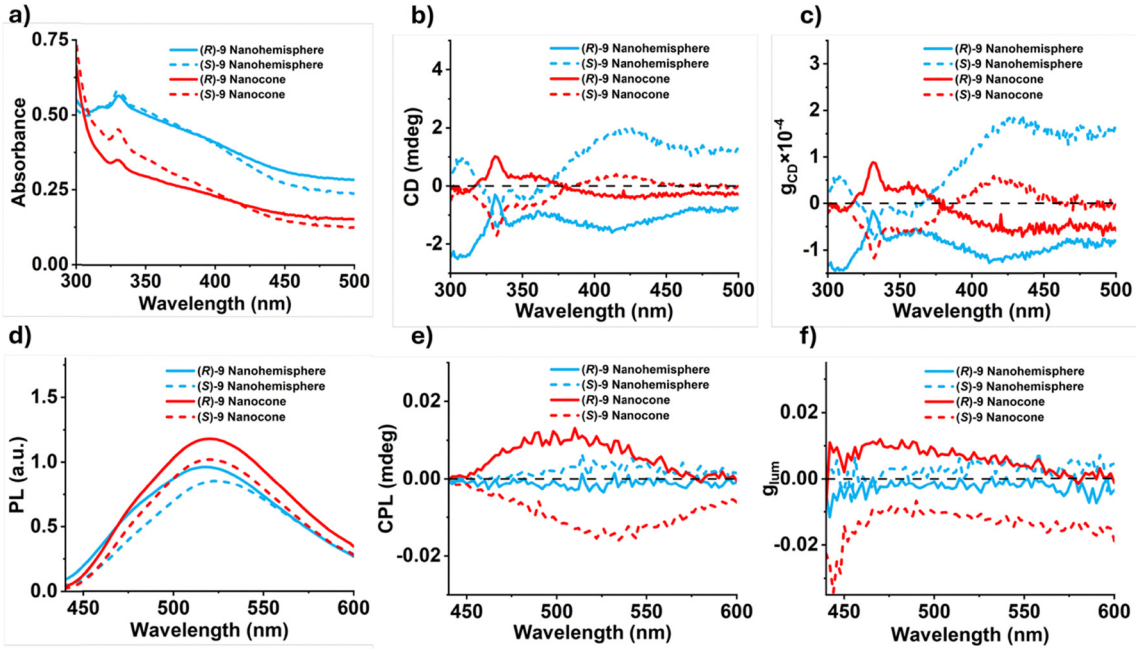

Fig. 4 (a) Electronic absorption spectra, (b) CD spectra, (c) absorption asymmetry factor (g_{CD}), (d) PL spectra (λ_{ex} = 320 nm), (e) CPL spectra, and (f) luminescence dissymmetry factor (g_{lum}) of the nanohemispheres and nanocones of (*R*) and (*S*)-**9**.

Subsequently, the photoluminescence spectra of these nanostructures were measured. Upon excitation at 320 nm, all of them exhibited strong emission, as shown in Fig. 4d. However, only the nanocones displayed a pronounced CPL signal (Fig. 4e). This comparison indicates that neither efficient luminescence nor ground-state chirality alone is sufficient to generate CPL generation; instead, a chiral excited-state organization is required. The g_{lum} value of the nanocones was determined to be approximately 0.01 (Fig. 4f), which is significantly higher than those reported for some TADF-based systems[57–59] and lipid-based assemblies,[21,30] and is comparable to that of the chiral π-gelator reported by Yang *et al.* (1.1×10^{-2}).[60] These results collectively suggest that the nanocones support a chiral excited state, whereas the nanohemispheres, despite being chiral in the ground state, do not effectively translate this chirality into the emissive excited state.

To rationalize the distinct CPL activities of the three nanostructures, the role of exciton coupling between closely packed chromophores is considered. Exciton coupling typically arises when transition dipoles interact in a chiral arrangement, often manifested as bisignate CD signals.[61] For the nanotubes of (*R*)- and (*S*)-**9**, although pronounced CD signals are observed, the spectra are dominated by the higher-energy band (~355 nm) with relatively weak contribution from the lower-energy CT band (~420 nm). This behavior is consistent with transitions of mixed LE/CT character with limited conjugation. The absence of clear bisignate features suggests that excitonic interactions are weak, likely due to insufficient electronic coupling between carbazole units. Consequently, the excited states remain only weakly chiral, leading to negligible CPL activity.

In the case of nanohemispheres, the CD spectra are dominated by a strong, non-sign-inverting band at ~420 nm, indicative of a more delocalized CT state. While this suggests enhanced donor–acceptor conjugation, the lack of bisignate CD features implies limited exciton coupling between chromophores. The excited states are therefore not effectively organized into a chiral excitonic manifold, resulting in weak CPL.

In contrast, the nanocones exhibit mirror-symmetric, bisignate CD signals spanning 350–450 nm, characteristic of strong exciton coupling. This indicates a chiral arrangement of interacting transition dipoles, consistent with a helical supramolecular organization. Such coupling enables the formation of chiral excited states, thereby giving rise to pronounced CPL activity.

Conclusions

In summary, we have reported a simple molecular design of luminophore–lipid conjugates that contains one lipid chain, one polar head, one chiral center, and one luminophore. By using glycerolipids, a typical class of chiral lipids, as the backbone and Cz_3PN as the luminophore, the resulting conjugates exhibited different self-assembly properties under different conditions mainly due to the lipid polymorphism. Interestingly, on a polar glass surface, molecules of the enantiomeric (*R*) and (*S*)-**9** underwent self-assembly to form nanocones with a diameter of approximately 400–600 nm and a height of 80–100 nm as determined by AFM. These nanostructures exhibited mirror-symmetric Cotton effects in their CD spectra and notable CPL signals with a high luminescence dissymmetry factor of 0.01. These simple molecular and supramolecular designs could facilitate further study of the structure–activity relationship in self-assembled CPL-active

nanostructures that could improve their performance for practical applications.

Author contributions

C. L. performed experiments, conducted data analysis, and wrote the original draft. X. C. and Z. H. supported the CD and CPL measurements. Q. Z. analyzed the data and wrote the original draft. Z. L. and L. J. recorded the cryo-TEM images. D. K. P. N. provided resources, supervised the project, and reviewed and edited the manuscript. All authors helped to improve the manuscript.

Conflicts of interest

There are no conflicts to declare.

Data availability

The data supporting this article have been included in the supplementary information (SI). Supplementary information: experimental details, chromatograms of a mixture of (*R*) and (*S*)-**9**, (*R*)-**9**, and (*S*)-**9**, spectral data of (*R*) and (*S*)-**9** in DMF, hydrodynamic diameter distribution of the nanotubes of (*R*) and (*S*)-**9**, statistical analyses of the AFM images and Raman spectra of the nanocones and nanohemispheres of (*R*) and (*S*)-**9**, and NMR and mass spectra of all new compounds. See DOI: **https://doi.org/10.1039/**d6qm00159a.

Acknowledgements

This work was supported by a Collaborative Research Fund from the Research Grants Council of the Hong Kong Special Administrative Region, China (ref. no. C4057-24GF).

References

1 Z.-L. Gong, X. Zhu, Z. Zhou, S.-W. Zhang, D. Yang, B. Zhao, Y.-P. Zhang, J. Deng, Y. Cheng, Y.-X. Zheng, S.-Q. Zang, H. Kuang, P. Duan, M. Yuan, C.-F. Chen, Y. S. Zhao, Y.-W. Zhong, B. Z. Tang and M. Liu, Frontiers in circularly polarized luminescence: molecular design, self-assembly, nanomaterials, and applications, *Sci. China: Chem.*, 2021, **64**, 2060–2104.

2 Y. Zhang, S. Yu, B. Han, Y. Zhou, X. Zhang, X. Gao and Z. Tang, Circularly polarized luminescence in chiral materials, *Matter*, 2022, **5**, 837–875.

3 F. Furlan, J. M. Moreno-Naranjo, N. Gasparini, S. Feldmann, J. Wade and M. J. Fuchter, Chiral materials and mechanisms for circularly polarized light-emitting diodes, *Nat. Photonics*, 2024, **18**, 658–668.

4 P. Stachelek, S. Serrano-Buitrago, B. L. Maroto, R. Pal and S. de la Moya, Circularly polarized luminescence bioimaging using chiral BODIPYs: A model scaffold for advancing unprecedented CPL microscopy using small full-organic probes, *ACS Appl. Mater. Interfaces*, 2024, **16**, 67246–67254.

5 L. E. MacKenzie and R. Pal, Circularly polarized lanthanide luminescence for advanced security inks, *Nat. Rev. Chem.*, 2021, **5**, 109–124.

6 S.-Y. Li, Y. Zong, B.-H. Liu, N. Liu and Z.-Q. Wu, Helix-induced full-color circularly polarized luminescence films with multiple information encryption and multi-stimuli responsiveness, *Chem. Sci.*, 2025, **16**, 5036–5042.

7 Z. Feng, J. Li, P. Yang, X. Xu, D. Wang, J. Li, C. Zhang, J. Li, H. Zhang, G. Zou and X. Chen, Dynamic multimodal information encryption combining programmable structural coloration and switchable circularly polarized luminescence, *Nat. Commun.*, 2025, **16**, 2264.

8 G. Yang, L. Zhu, J. Hu, H. Xia, D. Qiu, Q. Zhang, D. Zhang and G. Zou, Near-infrared circularly polarized light triggered enantioselective photopolymerization by using upconversion nanophosphors, *Chem. – Eur. J.*, 2017, **23**, 8032–8038.

9 C. He, Z. Feng, S. Shan, M. Wang, X. Chen and G. Zou, Highly enantioselective photo-polymerization enhanced by chiral nanoparticles and in situ photopatterning of chirality, *Nat. Commun.*, 2020, **11**, 1188.

10 E. M. Sánchez-Carnerero, A. R. Agarrabeitia, F. Moreno, B. L. Maroto, G. Muller, M. J. Ortiz and S. de al Moya, Circularly polarized luminescence from simple organic molecules, *Chem. – Eur. J.*, 2015, **21**, 13488–13500.

11 Y. Chen, Circularly polarized luminescence based on small organic fluorophores, *Mater. Today Chem.*, 2022, **23**, 100651.

12 D. Thakur and S. Vaidyanathan, Chirality inducing units in organic TADF molecules: a way to circularly polarized luminescence, *J. Mater. Chem. C*, 2024, **12**, 13168–13229.

13 T. Zhang, Y. Zhang, Z. He, T. Yang, X. Hu, T. Zhu, Y. Zhang, Y. Tang and J. Jiao, Recent advances of chiral isolated and small organic molecules: Structure and Properties for Circularly Polarized Luminescence, *Chem. – Asian J.*, 2024, **19**, e202400049.

14 J.-F. Chen, Q.-X. Gao, H. Yao, B. Shi, Y.-M. Zhang, T.-B. Wei and Q. Lin, Recent advances in circularly polarized luminescence of planar chiral organic compounds, *Chem. Commun.*, 2024, **60**, 6728–6740.

15 Y. Sang, J. Han, T. Zhao, P. Duan and M. Liu, Circularly polarized luminescence in nanoassemblies: Generation, amplification, and application, *Adv. Mater.*, 2020, **32**, 1900110.

16 B.-H. Liu, Y. Zong, N. Liu and Z.-Q. Wu, Advances in self-assembly-based circularly polarized luminescent materials, *Sci. China: Chem.*, 2024, **67**, 3247–3257.

17 K. Miki, T. Noda, M. Gon, K. Tanaka, Y. Chujo, Y. Mizuhata, N. Tokitoh and K. Ohe, Near-infrared circularly polarized luminescence through intramolecular excimer formation of oligo(*p*-phenyleneethynylene)-based double helicates, *Chem. – Eur. J.*, 2019, **25**, 9211–9216.

18 D. Hartmann, S. E. Penty, M. A. Zwijnenburg, R. Pal and T. A. Barendt, A bis-perylene diimide macrocycle chiroptical switch, *Angew. Chem., Int. Ed.*, 2025, **64**, e202501122.

19 H. Qu, Y. Wang, Z. Li, X. Wang, H. Fang, Z. Tian and X. Cao, Molecular face-rotating cube with emergent chiral and

fluorescence properties, *J. Am. Chem. Soc.*, 2017, **139**, 18142–18145.
20 Y. Wang, D. Niu, G. Ouyang and M. Liu, Double helical π-aggregate nanoarchitectonics for amplified circularly polarized luminescence, *Nat. Commun.*, 2022, **13**, 1710.
21 C. Du, Z. Li, X. Zhu, G. Ouyang and M. Liu, Hierarchically self-assembled homochiral helical microtoroids, *Nat. Nanotechnol.*, 2022, **17**, 1294–1302.
22 C. Du, X. Zhu, C. Yang and M. Liu, Stacked reticular frame boosted circularly polarized luminescence of chiral covalent organic frameworks, *Angew. Chem., Int. Ed.*, 2022, **61**, e202113979.
23 C. Vicente-Garcia and I. Colomer, Lipopeptides as tools in catalysis, supramolecular, materials and medicinal chemistry, *Nat. Rev. Chem.*, 2023, **7**, 710–731.
24 Y. Luo, A. B. Cook, L. K. E. A. Abdelmohsen and J. C. M. van Hest, Polymer vesicles and lipid nanoparticles, *Ann. Rev. Mater. Res.*, 2024, **54**, 75–96.
25 H. M. G. Barriga, M. N. Holme and M. M. Stevens, Cubosomes: The next generation of smart lipid nanoparticles?, *Angew. Chem., Int. Ed.*, 2019, **58**, 2958–2978.
26 H. Cao, Y. Yang and J. Li, AIEgen–lipid structures: Assembly and biological applications, *Aggregates*, 2020, **1**, 69–79.
27 R. Tenchov, R. Bird, A. E. Curtze and Q. Zhou, Lipid nanoparticles –From liposomes to mRNA vaccine delivery, a landscape of research diversity and advancement, *ACS Nano*, 2021, **15**, 16982–17015.
28 J. Gong, M. Yu, C. Wang, J. Tan, S. Wang, S. Zhao, Z. Zhao, A. Qin, B. Tang and X. Zhang, Reaction-based chiroptical sensing of ClO^- using circularly polarized luminescence *via* self-assembly organogel, *Chem. Commun.*, 2019, **55**, 10768–10771.
29 A. Mukherjee and S. Ghosh, Circularly polarized luminescence from chiral supramolecular polymer and seeding effect, *Chem. – Eur. J.*, 2020, **26**, 12874–12881.
30 Q. Cheng, A. Hao and P. Xing, A chemosensor-based chiral coassembly with switchable circularly polarized luminescence, *Nat. Commun.*, 2021, **12**, 6320.
31 K. Nakamura, H. Minami, A. Sagara, N. Itamoto and N. Kobayashi, Enhanced red emissions of europium(iii) chelates in DNA–CTMA complexes, *J. Mater. Chem. C*, 2018, **6**, 4516–4522.
32 A. Mukherjee, D. S. Pal, H. Kar and S. Ghosh, Confined supramolecular polymers in water with exceptional stability, photoluminescence and chiroptical properties, *Polym. Chem.*, 2020, **11**, 7481–7486.
33 X. Yang, X. Jin, L. Zhou, P. Duan, Y. Fan and Y. Wang, Modulating the excited state chirality of dynamic chemical reactions in chiral micelles, *Angew. Chem., Int. Ed.*, 2022, **61**, e202115600.
34 Q. Cheng, A. Hao and P. Xing, A chemosensor-based chiral coassembly with switchable circularly polarized luminescence, *Nat. Commun.*, 2021, **12**, 6320.
35 J. Zhang, A. Hao and P. Xing, Oxidation triggered supramolecular chirality, *Nano Lett.*, 2024, **24**, 16191–16199.
36 D. Yang, J. Han, Y. Sang, T. Zhao, M. Liu and P. Duan, Steering triplet–triplet annihilation upconversion through enantioselective self-assembly in a supramolecular gel, *J. Am. Chem. Soc.*, 2021, **143**, 13259–13265.
37 J. Han, S. Fujikawa and N. Kimizuka, Living hybrid exciton materials: Enhanced fluorescence and chiroptical properties in living supramolecular polymers with strong Frenkel/charge-transfer exciton coupling, *Angew. Chem., Int. Ed.*, 2024, **63**, e202410431.
38 J. Bocková, N. C. Jones, S. V. Hoffmann and C. Meinert, The astrochemical evolutionary traits of phospholipid membrane homochirality, *Nat. Rev. Chem.*, 2024, **8**, 652–664.
39 J. Buendía, E. E. Greciano and L. Sánchez, Influence of axial and point chirality in the chiral self-assembly of twin *N*-annulated perylenecarboxamides, *J. Org. Chem.*, 2015, **80**, 12444–12452.
40 F. Biedermann and H.-J. Schneider, Experimental binding energies in supramolecular complexes, *Chem. Rev.*, 2016, **116**, 5216–5300.
41 P. Walde and E. Blöchliger, Circular dichroic properties of phosphatidylcholine liposomes, *Langmuir*, 1997, **13**, 1668–1671.
42 Z. Yang, Z. Mao, Z. Xie, Y. Zhang, S. Liu, J. Zhao, J. Xu, Z. Chi and M. P. Aldred, Recent advances in organic thermally activated delayed fluorescence materials, *Chem. Soc. Rev.*, 2017, **46**, 915–1016.
43 M. A. Bryden and E. Zysman-Colman, Organic thermally activated delayed fluorescence (TADF) compounds used in photocatalysis, *Chem. Soc. Rev.*, 2021, **50**, 7587–7680.
44 S. D. Stamatov and J. Stawinski, Regioselective and stereospecific acylation across oxirane- and silyloxy systems as a novel strategy to the synthesis of enantiomerically pure mono-, di- and triglycerides, *Org. Biomol. Chem.*, 2007, **5**, 3787–3800.
45 A. Wannebroucq, R. Meunier-Prest, J.-C. Chambron, C.-H. Brachais, J.-M. Suisse and M. Bouvet, Synthesis and characterization of fluorophthalocyanines bearing four 2-(2-thienyl)ethoxy moieties: from the optimization of the fluorine substitution to chemosensing, *RSC Adv.*, 2017, **7**, 41272–41281.
46 Y. Wang and A. M. Chen, Enantioenrichment by crystallization, *Org. Process Res. Dev.*, 2008, **12**, 282–290.
47 K. Chu, Z. Ding and E. Zysman-Colman, Materials for electrochemiluminescence: TADF, hydrogen-bonding, and aggregation- and crystallization-induced emission luminophores, *Chem. – Eur. J.*, 2023, **29**, e202301504.
48 D. Regan, J. Williams, P. Borri and W. Langbein, Lipid bilayer thickness measured by quantitative DIC reveals phase transitions and effects of substrate hydrophilicity, *Langmuir*, 2019, **35**, 13805–13814.
49 X. Zhu, Y. Jiang, D. Yang, L. Zhang, Y. Li and M. Liu, Homochiral nanotubes from heterochiral lipid mixtures: a shorter alkyl chain dominated chiral self-assembly, *Chem. Sci.*, 2019, **10**, 3873–3880.
50 P. Li, B. Lü, D. Han, P. Duan, M. Liu and M. Yin, Stoichiometry-controlled inversion of circularly polarized luminescence in co-assembly of chiral gelators with an achiral tetraphenylethylene derivative, *Chem. Commun.*, 2019, **55**, 2194–2197.

51 C. Chen, Z. Chi, K. C. Chong, A. S. Batsanov, Z. Yang, Z. Mao, Z. Yang and B. Liu, Carbazole isomers induce ultralong organic phosphorescence, *Nat. Mater.*, 2021, **20**, 175–180.

52 A. Kumar, A. Saha, A. Kumar, P. Mandi and M. D. Choudhury, Tailoring the wettability and evaporation dynamics of polymeric surfaces via surface modifications, *Colloid Polym. Sci.*, 2025, **303**, 2389–2401.

53 D. Hussain, K. Ahmad, J. Song and H. Xie, Advances in the atomic force microscopy for critical dimension metrology, *Meas. Sci. Technol.*, 2017, **28**, 012001.

54 H. Noda, X.-K. Chen, H. Nakanotani, T. Hosokai, M. Miyajima, N. Notsuka, Y. Kashima, J.-L. Brédas and C. Adachi, Critical role of intermediate electronic states for spin-flip processes in charge-transfer-type organic molecules with multiple donors and acceptors, *Nat. Mater.*, 2019, **18**, 1084–1090.

55 Y. Shi, H. Ma, Z. Sun, W. Zhao, G. Sun and Q. Peng, Optimal dihedral angle in twisted donor–acceptor organic emitters for maximized thermally activated delayed fluorescence, *Angew. Chem., Int. Ed.*, 2022, **61**, e202213463.

56 H. S. Kim, S. H. Lee, S. Yoo and C. Adachi, Understanding of complex spin up-conversion processes in charge-transfer-type organic molecules, *Nat. Commun.*, 2024, **15**, 2267.

57 M. Li, Y.-F. Wang, D. Zhang, L. Duan and C.-F. Chen, Axially chiral TADF-active enantiomers designed for efficient blue circularly polarized electroluminescence, *Angew. Chem., Int. Ed.*, 2020, **59**, 3500–3504.

58 M. Li, M.-Y. Wang, Y.-F. Wang, L. Feng and C.-F. Chen, High-efficiency circularly polarized electroluminescence from TADF-sensitized fluorescent enantiomers, *Angew. Chem., Int. Ed.*, 2021, **60**, 20728–20733.

59 C. Shi, J.-M. Jin, R.-J. Wang, W.-C. Chen, C.-L. Sun, S. Ji, Y. Huo and H.-L. Zhang, Highly efficient narrowband circularly polarized luminescence from discrete supramolecular aggregates, *Adv. Mater.*, 2025, **37**, 2420611.

60 D. Yang, P. Duan, L. Zhang and M. Liu, Chirality and energy transfer amplified circularly polarized luminescence in composite nanohelix, *Nat. Commun.*, 2017, **8**, 15727.

61 N. Berova, N. Harada and K. Nakanishi, *Exciton coupling, in Encyclopedia of Spectroscopy and Spectrometry*, ed. J. C. Lindon, Academic Press, Oxford, 2nd edn, 1999, pp. 542–558.

